Letters

A Model-Independent Online Learning-Based Control Strategy for DC/AC Inverters

Zifan Lin, *Member, IEEE*, Yulin Liu, Wenxiang Du, *Graduate Student Member, IEEE*, Qingle Sun, Herbert Ho-Ching Iu, *Fellow, IEEE*, Tyrone Fernando, *Senior Member, IEEE*, and Xinan Zhang, *Senior Member, IEEE*

***Abstract*—This letter proposes a novel control scheme for power electronic inverters using a barrier Lyapunov function guided radial basis function neural network controller, featuring online learning and real-time applicability. Unlike many existing adaptive neural network-based controller, the proposed method requires no knowledge of system parameters and does not require any offline training. The control law is updated entirely online with guaranteed convergence, ensuring bounded current tracking under uncertainties and disturbances. Its simple structure leads to extremely low computational complexity, making it one of the most efficient model-free controller currently applicable to real-time dc–ac inverter control. The effectiveness and robustness of the proposed controller are verified through application to a three-level neutral-point-clamped inverter.**

***Index Terms*—Model independent, neural network, three-level neutral point clamped (3L-NPC) inverter.**

I. Introduction

DC/AC inverters have seen rapid development in recent years and are widely deployed in applications, such as solar photovoltaic systems [1], ship propulsion [2], and microgrids [3]. Numerous control strategies have been proposed to improve the performance of dc/ac inverters [4], [5], [6], [7], [8], [9], [10], [11]. For instance, finite control set model predictive control (MPC) [4], [5], [6], [7] has attracted significant attention due to its straight forward formulation and fast dynamic response; however, its dependence on precise system models limits robustness under parameter variations. A deadbeat predictive control in [8] also demonstrates good current quality and reliability. To overcome this, improved MPC methods have been developed, integrating observer-based parameter estimation methods, such as adaptive observer in [9] and refined extended state observer in [10], to enhance parameter adaptation and tracking performance. In addition, machine-learning-based controllers have emerged as promising solutions for complex or nonlinear system compensation, enabling real-time learning and control adjustment [11]. Despite their potential, most of these approaches still face challenges related to model dependence, computational complexity, or training requirements, which can hinder real-time implementation and widespread adoption in industrial applications.

To mitigate model dependence, Jin et al. [9] proposed an adaptive model predictive control, which employs an online adaptive observer to estimate system parameters. Unfortunately this method introduces extra observer gain tuning issue and suffers from high computational burden. In 2023, a deep deterministic policy gradient-assisted integral reinforcement learning controller with excellent performance was proposed in [11]. Yet, it requires the tuning of covariance matrix in its recursive least squares algorithm and imposes high computational cost.

To address the limitations of existing model-based and learning-based control methods, including sensitivity to parameter variations, requirement for accurate modeling, and excessive computational burden, this letter is motivated to develop a real-time applicable solution that ensures stability without relying on the knowledge of system model. The proposed controller features online learning, avoids offline training or parameter identification, and guarantees bounded tracking performance under uncertainties and disturbances. Its simplicity and low computational cost make it well suited for real-time implementation in power electronic systems, such as the dc/ac inverters.

II. System Modeling

A. Inverter Configuration

The topology used in this letter to verify the proposed controller is a three-level neutral point clamped (3L-NPC) inverter. The mathematical model of the 3L-NPC inverter in the stationary

Received 1 June 2025; revised 27 July 2025; accepted 26 August 2025. Date of publication 2 September 2025; date of current version 22 October 2025. This work was supported by Future Battery Industries CRC under Grant PG 55003300. *(Corresponding author: Xinan Zhang.)*

Zifan Lin, Yulin Liu, Wenxiang Du, Herbert Ho-Ching Iu, Tyrone Fernando, and Xinan Zhang are with the Department of Electrical and Electronic Engineering, University of Western Australia, Perth, WA 6009, Australia (e-mail: zifan.lin@research.uwa.edu.au; yulin.liu.ee@outlook.com; 23997355@student.uwa.edu.au; herbert.iu@uwa.edu.au; tyrone.fernando@uwa.edu.au; xinan.zhang@uwa.edu.au).

Qingle Sun is with the School of Mechanical Engineering, Beijing Institute of Technology, Beijing 100081, China (e-mail: sunqingle@bit.edu.cn).

Color versions of one or more figures in this article are available at https://doi.org/10.1109/TPEL.2025.3605559.

Digital Object Identifier 10.1109/TPEL.2025.3605559

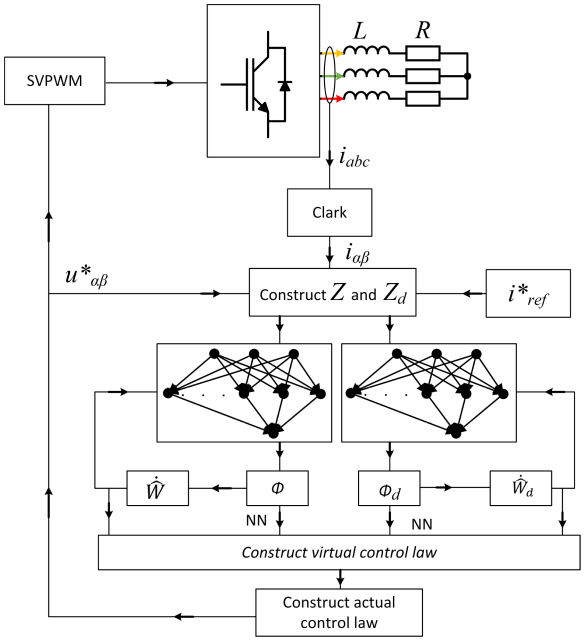

Fig. 1. Control block diagram for the proposed controller.

$\alpha\beta$-reference frame can be expressed as

$$u = L\dot{Y} + RY \tag{1}$$

where $u = \left[u^*_\alpha(t), u^*_\beta(t)\right]^T$ represents control input and desired voltage vector in $\alpha\beta$-reference frame, $Y = \left[i_\alpha(t), i_\beta(t)\right]^T$ denote system output and corresponding currents in $\alpha\beta$-axis. L and R represent the inductance and resistance of the load, respectively. Reconstructing $i_\alpha(t)$ and $i_\beta(t)$ into its second derivative term, the equation can be derived as follows:

$$u = \frac{R}{\omega^2}\ddot{Y} + L\dot{Y} \tag{2}$$

where ω is the angular frequency.

B. Problem Formulation

Taking model uncertainty and disturbance into account, (2) can be rewritten as

$$u = \Delta u + d = \frac{R}{\omega^2}\ddot{Y} + L\dot{Y} \tag{3}$$

where $\Delta = [\Delta_\alpha, \Delta_\beta](0 < \Delta_{\alpha,\beta} \leqslant 1)$ and d denotes the impact of model uncertainty and disturbance. Model uncertainty is considered to include inherent model uncertainties arising from device imperfections, temperature-induced variations, and operational parameter drift. The block diagram of the proposed method is shown in Fig. 1, which consists of two radial basis function neural networks (RBFNNs) with simple structure. Each RBFNN has three layers, i.e., input, hidden, and output layers. The disturbance $d(t)$ introduced in this letter is assumed to be continuous in time and bounded, which yields $\forall t > 0$, such that $d \leqslant \bar{d}$. The control objective is to ensure that output Y follows the desired reference trajectory Y_r while guaranteeing prescribed performance and the boundedness of all closed-loop signals.

III. Methodology

In the proposed control method, the following performance function is defined:

$$f(t) = (f_{\min} - f_{\max})\, e^{-th} + f_{\max} \tag{4}$$

where $f_{\min}, f_{\max}$, and h are positive constants to be designed. $f(t)$ and $\tau f(t)(0 \leqslant \tau < 1)$ constrain the initial error and the tracking error to be within the bounded region [12]. To achieve zero steady-state error, e and E are defined as

$$e = Y - Y_r = \begin{bmatrix} e_\alpha \\ e_\beta \end{bmatrix} E = \dot{e} + \lambda e = \begin{bmatrix} E_\alpha \\ E_\beta \end{bmatrix} \tag{5}$$

where λ is a positive diagonal matrix to be designed. As mentioned above, the achievement of prescribed performance can be transformed into the problem of finding the control gains subject to time-varying constraints. The upper and lower constraints of tracking error are expressed as $f(t) = \bar{U} = [\bar{U}_\alpha\ , \bar{U}_\beta]$ and $\tau f(t) = \underline{U} = [\underline{U}_\alpha\ , \underline{U}_\beta]$, respectively. Introducing a barrier Lyapunov function (BLF) as follows:

$$\begin{aligned} V_1 = &\left[\frac{I(e_\alpha)}{2}\ln\left(\frac{\bar{U}_\alpha^2}{\bar{U}_\alpha^2 - e_\alpha^2}\right) + \frac{1 - I(e_\alpha)}{2}\ln\left(\frac{\bar{U}_\alpha^2}{\bar{U}_\alpha^2 - e_\alpha^2}\right)\right] \\ &+ \left[\frac{I(e_\beta)}{2}\ln\left(\frac{\bar{U}_\beta^2}{\bar{U}_\beta^2 - e_\beta^2}\right)\right. \\ &\left. + \frac{1 - I(e_\beta)}{2}\ln\left(\frac{\underline{U}_\beta^2}{\underline{U}_\beta^2 - e_\beta^2}\right)\right] \end{aligned} \tag{6}$$

where $I(e_i)$ is an indicator function that equals to 1 if $e_i > 0$, and 0, otherwise. Differentiating $\dot{V}_1$ yields

$$\begin{aligned} \dot{V}_1 = \sum_{i=1}^{2}\Bigg\{ &\frac{I(e_i)\, e_i}{\bar{U}_i^2 - e_i^2}\left(E_i - \lambda_i e_i - e_i\frac{\dot{\bar{U}}_i}{\bar{U}_i}\right) \\ &+ \frac{(1 - I(e_i))\, e_i}{\underline{U}_i^2 - e_i^2}\left(E_i - \lambda_i e_i - e_i\frac{\dot{\underline{U}}_i}{\underline{U}_i}\right)\Bigg\}. \end{aligned} \tag{7}$$

The diagonal matrix λ_i is introduced as

$$\lambda_i = \kappa_{1i} + \delta_i \tag{8}$$

where κ_{1i} is a constant and δ_i is defined as an upper bound of

$$\begin{aligned} &\sqrt{\left(\frac{\dot{\bar{U}}_i}{\bar{U}_i}\right)^2 + \left(\frac{\dot{\underline{U}}_i}{\underline{U}_i}\right)^2} \\ &= \sqrt{2}h\left(\frac{f_{\min} - f_{\max}}{f_{\min} - f_{\max} + f_{\max}e^{lt}}\right) \\ &\leq \sqrt{2}h. \end{aligned} \tag{9}$$

Combining (7) with (9) yields

$$\begin{aligned} \dot{V}_1 \leq \sum_{i=1}^{2}\Bigg\{ &-\kappa_{1i}e_i^2\left(\frac{I(e_i)}{\bar{U}_i^2 - e_i^2} + \frac{1 - I(e_i)}{\underline{U}_i^2 - e_i^2}\right) \\ &+ E\left(\frac{I(e_i)e_i}{\bar{U}_i^2 - e_i^2} + \frac{(1 - I(e_i))e_i}{\underline{U}_i^2 - e_i^2}\right)\Bigg\} \end{aligned}$$

$$\leq \sum_{i=1}^{2} \left(-\kappa_{1i} e_i z_{1i} + E^T z_{1i}\right) \tag{10}$$

where $z_{1i} = [z_{11}, z_{12}]$ is an auxiliary variable vector, which is defined as

$$z_{1i} = \frac{I(e_i)\, e_i(t)}{{U_{\text{top}}}^2(t) - {e_i}^2(t)} + \frac{(1 - I(e_i))\, e_i(t)}{{U_{\text{bot}}}^2(t) - {e_i}^2(t)}. \tag{11}$$

Introducing a new Lyapunov function

$$V_2 = V_1 + \frac{1}{2} E^T \frac{R}{\omega^2} E. \tag{12}$$

Differentiating V_2 yields

$$\begin{aligned} \dot{V}_2 &= \dot{V}_1 + \frac{1}{2} E^T \frac{\dot{R}}{\omega^2} E + E^T \frac{R}{\omega^2} \dot{E} \\ &= \dot{V}_1 + \frac{1}{2} E^T \frac{\dot{R}}{\omega^2} E + E^T \frac{R}{\omega^2} \lambda \dot{e} - E^T \frac{R}{\omega^2} \ddot{Y}_r \\ &\quad + E^T (\Delta u + d) - E^T L \dot{Y} \\ &= \dot{V}_1 + E^T \left(\Delta u + d - L\dot{Y}_r - \frac{R}{\omega^2} \ddot{Y}_r + L\lambda e + \frac{R}{\omega^2} \lambda \dot{e}\right). \end{aligned} \tag{13}$$

Define two RBFNNs to estimate system uncertainties

$$W^T \Phi(Z) = -L\dot{Y}_r - \frac{R}{\omega^2} \ddot{Y}_r + L\lambda e + \frac{R}{\omega^2} \lambda \dot{e} + \alpha(Z) \tag{14}$$

$$W_d^T \Phi_d(Z_d) = \Delta u - L\dot{Y} + \alpha_d(Z_d) \tag{15}$$

where $Z = [Y^T, \dot{Y}^T, E^T]$ and $Z_d = [Y^T, \dot{Y}^T, u^T]$ are the RBF neural networks inputs, $\Phi(Z) = [\Phi_1(Z), \Phi_2(Z), \ldots, \Phi_n(Z)]^T$ and $\Phi_\sigma(Z_\sigma) = [\Phi_{d1}(Z_d), \Phi_{d2}(Z_d), \ldots, \Phi_{dn}(Z_d)]^T$ are the Gaussian RBFs, $\Phi_d(Z_d)$ satisfies $\|\Phi_d(Z_d)\| \leqslant \psi_d$ with ψ_d being an unknown positive constant, n is the hidden node number, W and W_d are the weights of the two neural networks, and $\alpha(Z)$ and $\alpha_d(Z_d)$ are the neural networks' approximation errors that satisfy $|\alpha(Z)| \leqslant \bar{\alpha}(Z)$ and $|\alpha_d(Z_d)| \leqslant \bar{\alpha}(Z)$, respectively. The weight updating laws of the neural networks are set as

$$\dot{\hat{W}} = -K \left(\Phi(Z) E + \varepsilon \hat{W}\right) \tag{16}$$

$$\dot{\hat{W}}_d = -K_d \left(\Phi_d(Z_d)\, \hat{d} + \varepsilon_d \hat{W}_d\right) \tag{17}$$

where K and K_d are the constant gain matrices; $\hat{d}$ is the approximation value of the disturbance; $\hat{W}$ and $\hat{W}_d$ are the estimations of the two weights; ε and ε_σ are small constants to avoid the drift of $W^T \Phi(Z)$ and $W_d^T \Phi_d(Z_d)$, respectively. Introducing an auxiliary variable z_2, the disturbance observer is constructed as

$$\hat{d} = \hat{z}_2 + \Gamma_d \dot{Y} \tag{18}$$

$$\dot{z}_2 = -\Gamma z_2 - \Gamma \left(\hat{W}_d^T \Phi_d(Z_d) + \Gamma_d \dot{Y}\right) \tag{19}$$

where Γ and Γ_d are diagonal matrices satisfying $\Gamma \geqslant a\Gamma_d \geqslant \Gamma_d A^{-1} > 0$ with a denoting the upper bound of the eigenvalues of A^{-1}. Then, substituting (32) into (31) and calculating the derivative of (31) yields

$$\dot{\hat{d}} = -\Gamma \hat{d} - \Gamma_d A^{-1} d - \Gamma \hat{W}_d^T \Phi_d(Z_d) + \Gamma_d A^{-1} \hat{W}_d^T \Phi_d(Z_d). \tag{20}$$

Applying Young's inequality, we conclude that

$$\dot{\hat{d}}^T \dot{\hat{d}} \leqslant -\dot{\hat{d}}^T \Gamma \dot{\hat{d}} - \dot{\hat{d}}^T \Gamma_d A^{-1} d + \left|\dot{\hat{d}}^T \Gamma \hat{W}_d^T \Phi_d(Z_d)\right| \tag{21}$$

$$\leqslant -\dot{\hat{d}}^T \left(\Gamma - \frac{1}{2} A^{-1} \Gamma - I\right) \dot{\hat{d}} + \frac{1}{2} \bar{d}^T a \Gamma \bar{d} \tag{22}$$

$$+ \frac{1}{2} \tilde{\alpha}_d^T(Z_d)\, \Gamma^2 \tilde{\alpha}_d(Z_d) + \frac{1}{2} \psi_d \|\Gamma W_d\|^2 \tag{23}$$

where I denotes the identity matrix. Then, the virtual control law ξ can be constructed as

$$\xi = \kappa_2 E + \hat{W}^T \Phi(Z) + z_2 - \hat{d}. \tag{24}$$

Thus, the model-free control law is solved as

$$u = -\hat{\phi} \xi \tag{25}$$

$$\dot{\hat{\phi}} = E u_v - k \hat{\phi}. \tag{26}$$

Note that the control laws in (25) and (26) is obtained without any knowledge of the system model and parameters.

TABLE I
EXECUTION TIME OF METHODS

Methods	Method 1 from [9]	Method 2 from [11]	Proposed method
Execution time (μs)	76.7	10,174.65	59.75

IV. EXPERIMENTAL RESULTS

To validate the effectiveness of the proposed control strategy, experiments are carried out on a 3L-NPC inverter. The proposed control strategy is implemented on the NXP QorlQ P5020 processor within the dSPACE DS1202 MicrolabBox, operating with a control cycle of 100 μs.

A. Computational Burden

The computational burden of proposed method is tested and compared with state-of-art and conventional methods. The control algorithms are implemented on a DSP TMS320F28335 processor, operating at a clock frequency of 150 MHz. A digital output port is used to measure execution time, where the output level is set to 5 V when the algorithm begins execution and reset to 0 V upon completion. This method provides an accurate assessment of the computational burden associated with each control scheme. The results of the computational performance analysis are presented in Table I.

The proposed method reduces the execution time by 99.41% compared to online learning-based method with neural network proposed in [11], and 22.1% compared to nonneural network observer-based adaptive control in [9]. This is mainly attributed to the efficient handling of the learning process and neural network due to the presence of prescribed performance function setting.

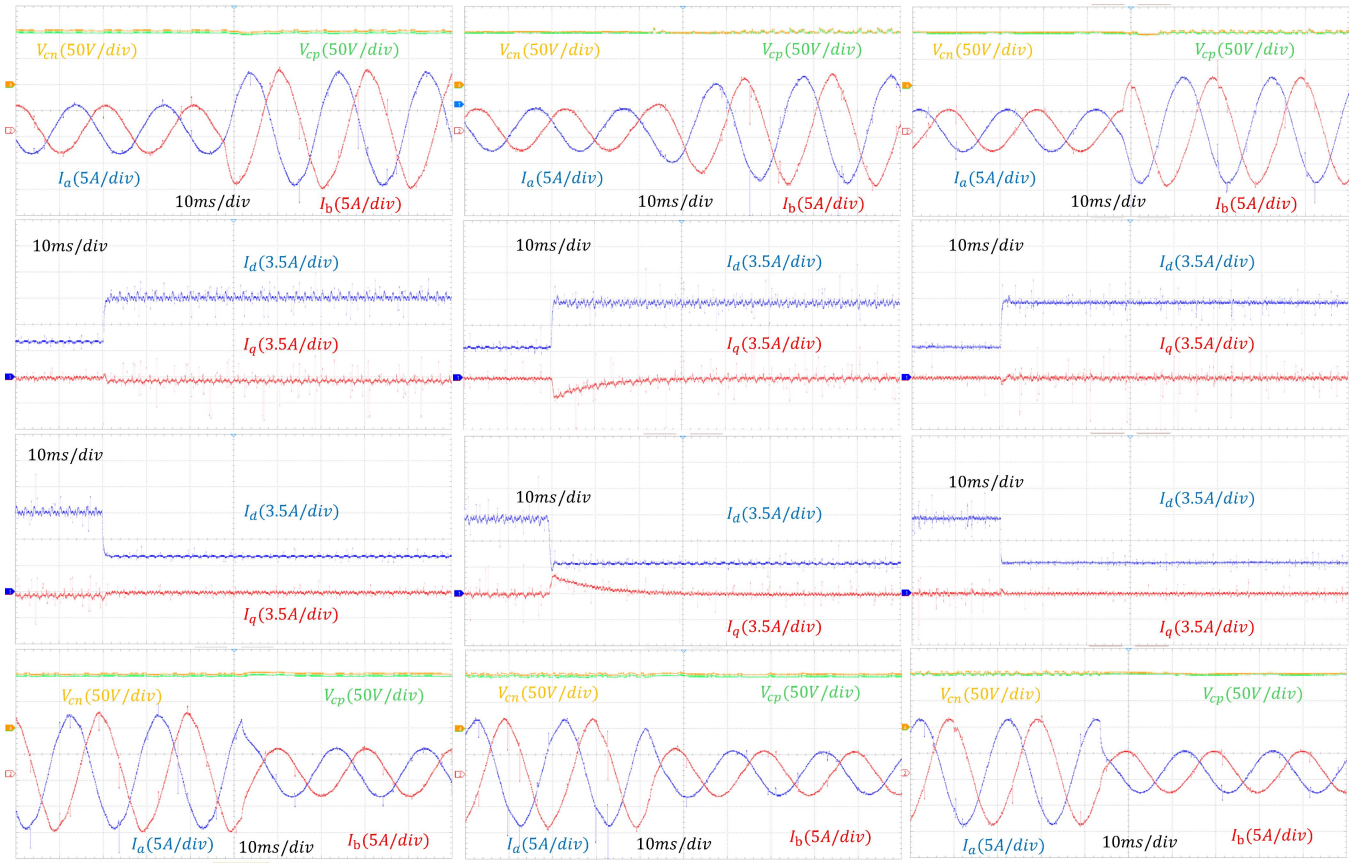

Fig. 2. Dynamic performance comparison under load step $I_d = 4$ A to $I_d = 10$ A then back to $I_d = 4$ A for (a) method 1 from [9], (b) method 2 from [11], and (c) proposed method.

B. Performance Comparison

The dynamic performance of proposed method is compared with method 1 from [9] and method 2 from [11] under a step change in current reference, where I_d transitions from 4 A to 10 A and is restored to 4 A. The experimental results are shown in Fig. 2. As illustrated, the proposed controller exhibits shorter settling time, smaller overshoot, and comparable neutral-point voltage performance compared to the other methods. In contrast, method 1 from [9] shows noticeable oscillations following the step change, and method 2 from [11] suffers from a longer transient period. The superior transient tracking capability confirms the effectiveness of the proposed control scheme under abrupt load variations.

The steady-state response of proposed controller, including the line currents I_a and I_b, and voltages across both the upper and lower capacitors V_{C1} and V_{C2}, are presented in Fig. 3. It can be seen that the proposed controller achieves excellent performance with a smooth current waveform. The total harmonic distortion of line current I_b is measured at 3.59% where d-axis current in the rotating reference frame $I_d = 4$ for proposed method, and 2.38% at $I_d = 10$. The prescribed performance is always obtained within the prescribed bounds.

To assess the thermal behavior of each control strategy, the inverter hardware was operated continuously for 60 min under two state-of-art methods and the proposed method, respectively.

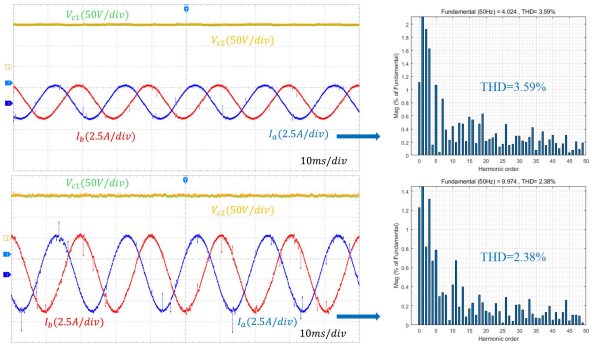

Fig. 3. Steady-state experiment result of $I_d = 4$ A and $I_d = 10$ A for the proposed method.

Fig. 4 presents the infrared thermal images captured at the start and the end of each test. The proposed method exhibits similar or slightly lower thermal buildup compared to method 1 from [9], while significantly outperforming the method 2 from [11], which shows elevated hot spots exceeding 41 °C. These results indicate that the proposed controller not only achieves fast and accurate current regulation but also minimizes thermal stress on the power devices during extended operation.

The proposed controller achieves precise current tracking and strong robustness against abrupt reference variations. Furthermore, its structurally simple and computation-efficient design

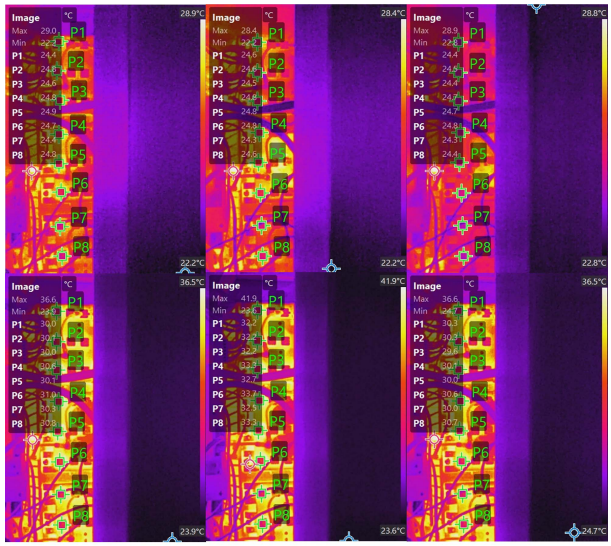

(a) AMPC (b) IRL (c) Proposed Method

Fig. 4. Infrared thermal images of the inverter hardware after 60 min of operation under (a) method 1 from [9], (b) method 2 from [11], and (c) proposed method.

facilitates real-time implementation on resource-constrained hardware platforms, thereby enhancing its practicality and deployment potential in industrial applications. Experimental validation includes comprehensive comparisons in terms of computational execution time, steady-state performance, transient response, and thermal profile. These results collectively confirm the proposed method's effectiveness and practical feasibility under various operating conditions.

V. Conclusion

This letter presents a computational efficient BLF-guided online learning controller for current regulation in dc/ac inverters. The proposed controller operates in a model-free manner, requiring no prior knowledge of inverter parameters or tedious offline training of neural network, and is capable of online learning with provable convergence within prescribed time and boundary conditions. This approach offers a promising and practical solution for intelligent control in advanced power electronic systems.

References

[1] G. H. B. Foo, T. Ngo, X. Zhang, and M. F. Rahman, "SVM direct torque and flux control of three-level simplified neutral point clamped inverter fed interior pm synchronous motor drives," *IEEE/ASME Trans. Mechatron.*, vol. 24, no. 3, pp. 1376–1385, Jun. 2019.

[2] F. Wang, Z. Li, and X. Tong, "Modified predictive control method of three-level simplified neutral point clamped inverter for common-mode voltage reduction and neutral-point voltage balance," *IEEE Access*, vol. 7, pp. 119476–119485, 2019.

[3] Q. Tabart, I. Vechiu, A. Etxeberria, and S. Bacha, "Hybrid energy storage system microgrids integration for power quality improvement using four-leg three-level NPC inverter and second-order sliding mode control," *IEEE Trans. Ind. Electron.*, vol. 65, no. 1, pp. 424–435, Jan. 2018.

[4] Y. Yang, H. Wen, M. Fan, M. Xie, and R. Chen, "Fast finite-switching-state model predictive control method without weighting factors for t-type three-level three-phase inverters," *IEEE Trans. Ind. Informat.*, vol. 15, no. 3, pp. 1298–1310, Mar. 2019.

[5] J.-H. Lee, J.-S. Lee, H.-C. Moon, and K.-B. Lee, "An improved finite-set model predictive control based on discrete space vector modulation methods for grid-connected three-level voltage source inverter," *IEEE Trans. Emerg. Sel. Topics Power Electron.*, vol. 6, no. 4, pp. 1744–1760, Dec. 2018.

[6] Q. Sun, Z. Lin, Z. Wang, H. H. C. Iu, T. Fernando, and X. Zhang, "Finite-set model predictive control with virtual medium voltage vectors and eliminated weighting factors for 3l-NPC inverters," *IEEE Trans. Ind. Electron.*, vol. 72, no. 7, pp. 7072–7083, Jul. 2025.

[7] X. Zhang, Z. Ma, X. Cai, X. Wu, Y. Han, and G. Lin, "Enhanced accuracy finite-control-set model-predictive control for three-phase three-level NPC inverter," *IEEE Trans. Power Electron.*, vol. 40, no. 8, pp. 10330–10334, Aug. 2025.

[8] Y. Jiang, C. Qin, X. Xing, X. Li, and C. Zhang, "A hybrid passivity-based control strategy for three-level T-type inverter in LVRT operation," *IEEE Trans. Emerg. Sel. Topics Power Electron.*, vol. 8, no. 4, pp. 4009–4024, Dec. 2020.

[9] F. Jin et al., "A novel adaptive model predictive current control for three-level simplified neutral-point-clamped inverter with carrier-based modulation," *IEEE Trans. Power Electron.*, vol. 40, no. 5, pp. 6593–6604, May 2025.

[10] Y. Zhang, J. Jin, and L. Huang, "Model-free predictive current control of PMSM drives based on extended state observer using ultralocal model," *IEEE Trans. Ind. Electron.*, vol. 68, no. 2, pp. 993–1003, Feb. 2021.

[11] C. Xiang et al., "A novel deep deterministic policy gradient assisted learning-based control algorithm for three-phase DC/AC inverter with an RL load," *IEEE Trans. Emerg. Sel. Topics Power Electron.*, vol. 11, no. 6, pp. 5529–5539, Dec. 2023.

[12] C. P. Bechlioulis and G. A. Rovithakis, "Robust adaptive control of feedback linearizable MIMO nonlinear systems with prescribed performance," *IEEE Trans. Autom. Control*, vol. 53, no. 9, pp. 2090–2099, Oct. 2008.